Exploration of the key parameters in sol-gel preparation of Ta_2O_5 films with high laser damage resistance

DI LIN[a], CHENG XU[a,*], MING MA[a], WEITONG SHAN[a], PEIZHONG FENG[a], DAWEI LI[b]
[a]*School of Materials Science and Engineering, China University of Mining and Technology, Xuzhou 221116, China*
[b]*Key Laboratory of High Power Laser Materials, Shanghai Institute of Optics and Fine Mechanics, Chinese Academy of Sciences, Shanghai 201800, China*

Ta_2O_5 films were prepared by using $TaCl_5$ as the precursor with different contents of H_2O_2, HNO_3 and acetylacetone (ACAC). The particle size, photoluminescence spectra and optical transmittance of the sols, as well as the surface morphology, weak absorption, laser-induce damage threshold (LIDT) and damage morphology of the films were studied. It was shown that the hydrolysis process in the sol was very slow when H_2O_2 was absent. With the H_2O_2 content increase, the nanoparticles grew faster in the sol. However, with the HNO_3 content increase, the hydrolysis process decreased and the sol became stable. The ACAC showed the inhibition effect similar to that of HNO_3 on the sol evolution. With the ACAC content increase, the LIDT of the films decreased after the first rising, which showed an opposite trend compared with the weak absorption. Moreover, based on the experimental results, a pseudo-ternary phase diagram of H_2O_2-HNO_3-ACAC system was proposed that is helpful for the high LIDT Ta_2O_5 film preparation.

(Received January 7, 2017; accepted June 7, 2017)

Keywords: Ta_2O_5, Hydrolysis, Absorption, Laser damage

1. Introduction

The optical components in the high-power laser system are always damaged under the action of laser, which in turn leads to the failure of the whole laser system. Therefore, the exploration of the laser damage mechanism in the optical components, especially that of the most easily damaged optical films which consequently increase their laser-induced damage threshold (LIDT), is significant to improve the performance of the laser system [1-4]. As one of the most important optical materials with large refractive index and low absorption in a wide wavelength range, Ta_2O_5 has extensively used in various optical films such as anti-reflection coatings, high-reflection coatings, interference filters and so on [5-7]. Meanwhile, since Ta_2O_5 has high laser damage resistance, it has attracted much attention in the application of laser films in recent years [8].

Nowadays, electron beam evaporation, magnetron sputtering and ion beam sputtering are the common physical vapor deposition (PVD) methods for the preparation of optical films [9-13]. However, Ta_2O_5 films prepared by PVD methods require more sophisticated equipments with relatively low LIDT [14-15]. Compared to PVD methods, the sol-gel technique is a chemical method with mild preparation conditions as well as simple process. Moreover, the sol-gel films tend to obtain higher LIDT than that of PVD films. Previous studies revealed that the films of low-refractive index material SiO_2 as well as most of the high-refractive index materials, such as TiO_2, ZrO_2 and HfO_2, prepared via the sol-gel method had very high LIDT [16-18]. In conventional sol-gel methods, tantalum alkoxides like tantalum ethoxide are always used as the precursors [19]. However, tantalum alkoxides are very expensive and unstable, which may seriously dampen researcher enthusiasm and restrict Ta_2O_5 film application to some extent. For this reason, using $TaCl_5$, which is much cheaper and more stable than tantalum alkoxides, as the precursor to prepare Ta_2O_5 film, is an ideal alternative solution. It is a pity that only in few studies $TaCl_5$ was used as a precursor in the Ta_2O_5 film preparation. In previous researches, we put forward an idea of using $TaCl_5$ as the precursor to prepare Ta_2O_5 films, which turned out to have high laser damage resistance [20]. Nevertheless, there is still a lack of in-depth understanding of the key parameters in the sol-gel Ta_2O_5 films preparation process.

In this paper, Ta_2O_5 films were prepared using $TaCl_5$ as a precursor in combination with different contents of key other reagents including H_2O_2, HNO_3 and acetylacetone (ACAC). The particle size, photo-luminescence spectra and optical transmittance of the sols, as well as the surface morphology, weak absorption, LIDT level and damage morphologies of the films were studied. Furthermore, a pseudo-ternary phase diagram of H_2O_2-HNO_3-ACAC system for preparing Ta_2O_5 films was proposed, which will better our understanding of the preparation process and obtain Ta_2O_5 films with high laser

damage resistance.

2. Experimental

Tantalum chloride (99.99%), ethanol (99.8%) and acetylacetone (99%) were purchased from Sigma-Aldrich. HNO_3 (70%) and H_2O_2 (30 wt. % in H_2O) were purchased from Sinopharm Chemical Reagent Co., Ltd in China. All reagents were used as received without further purification. To prepare Ta_2O_5 sols, three grams of $TaCl_5$ was firstly dissolved in 50 ml ethanol. Then, after vigorous stirring at room temperature, HNO_3, ACAC or H_2O_2 were added by drops to the above solution with a burette under stirring. Finally, the solution was sealed in a glass container and aged at 276 K for a minimum of 6 days to form the sols. With the change of H_2O_2, HNO_3 and ACAC content, eleven groups of the samples were synthesized, as shown in Table 1.

Table 1. The contents of H_2O_2, HNO_3 and ACAC in the samples

Groups No.	Sample	V_{H2O2} (ml)	V_{HNO3} (ml)	V_{ACAC} (ml)
1	H_2O_2-0	0	0.89	0.76
2	H_2O_2-0.35	0.35		
3	H_2O_2-0.71	0.71		
4	H_2O_2-0.91	0.91		
5	HNO_3-0	0.71	0	
(3)	HNO_3-0.89		0.89	
6	HNO_3-1.35		1.35	
7	HNO_3-1.94		1.94	
8	HNO_3-2.82		2.82	
9	ACAC-0		1.35	0
(6)	ACAC-0.76			0.76
10	ACAC-1.36			1.36
11	ACAC-1.45			1.45

Before Ta_2O_5 films preparation, BK7 substrates were carefully cleaned with ethanol under ultrasonic stimulation. The substrates were dip-coated at 60 mm/min using the prepared sols and, then, the deposited films were heated at 373 K for 10 min. The coating/heating cycles were repeated until the desired film thickness was reached.

The particle sizes of the sols were characterized by a JEOL-2010 transmission electron microscope (TEM). Photoluminescence spectra of the sols were measured by a Cary 3000 fluorescence spectrophotometer equipped with the laser excitation at 310 nm. The sol transmittance was measured at 500 nm using a Lambda 900 spectrophotometer. The Surface morphology and topography of the films were characterized by a Leica DMRXE optical microscopy and Dimension V atomic force microscopy (AFM), respectively. The root mean square (RMS) roughness was calculated from the AFM images. The weak absorption of the films was measured using the surface thermal lensing (STL) method [21]. Damage testing of the films was carried out in the "1-on-1" regime according to ISO standard 11254-1, using 1064 nm Q-switch pulsed laser at the pulse length of 12 ns [22-23]. Damage morphology after laser irradiation of the films was evaluated by a Sirion 200 field emission scanning electron microscope (FESEM).

3. Results and discussion

Since $TaCl_5$ is very stable, H_2O_2 is used in this study to accelerate the nucleation process in the sol. There are two important functions when using H_2O_2 as hydrolysis catalyst: (1) reduction of the concentration of Cl in the sol by oxidation of HCl into chlorine, and (2) generation of tantalum peroxide nanoparticles by reacting directly with $TaCl_5$ [6]. Therefore, the higher the H_2O_2 content induces faster nucleation process and bigger nanoparticles grown in the sol. The TEM images of Ta_2O_5 sols with different H_2O_2 contents are shown in Fig. 1. Fig. 1(a) shows a lot of organics in the sol. Fig. 1(b) shows some nanoparticles with uneven sizes. The reason can be attributed to the insufficient amount of H_2O_2, resulting in the relatively slow nucleation of a part of nanoparticles. Fig. 1(c) shows that with the increase of H_2O_2 concentration, the nanoparticles grow bigger and the size is uniform. Fig. 1(d)

shows that the larger size of nanoparticles appearing in the sol is due to the over growth of some nanoparticles because of the excessive content of H_2O_2. Simultaneously, milky opacity can be found in the sol by naked eye.

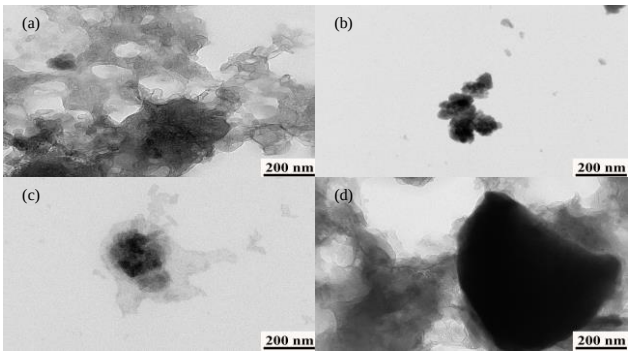

Fig. 1. TEM images of the sols (a) H_2O_2-0, (b) H_2O_2-0.35, (c) H_2O_2-0.71 and (d) H_2O_2-0.91

Fig. 2 shows the optical features in the films. Fig. 2(a) displays a large dendritic defect with the rings in the center on the film surface when H_2O_2 is not added. The stability of $TaCl_5$ leads to the slow hydrolysis process in the sol when H_2O_2 is absent. It makes the nucleation in the sol difficult, which in turn destroys the possibility of the film preparation. When the H_2O_2 content increases to 0.35, Fig. 2(b) shows that the film is formed although there are many elliptical granular defects on the surface. It indicates that the hydrolysis of $TaCl_5$ accelerates with the increase of H_2O_2 content in the sol. However, the hydrolysis is still insufficient due to the low H_2O_2 concentration, resulting in the granular defects appeared on the films surface. When the H_2O_2 content increases to 0.71, Fig. 2(c) shows that the film surface is smooth and free of defects. However, when the H_2O_2 content increases further to 0.91, many stripes emerge on the film surface, as is shown in Fig. 2(d). Due to the high H_2O_2 concentration and fast hydrolysis of $TaCl_5$, some larger nanoparticles are formed in the sol, as proved by Fig. 1(d), resulting in the nonuniform film surfaces.

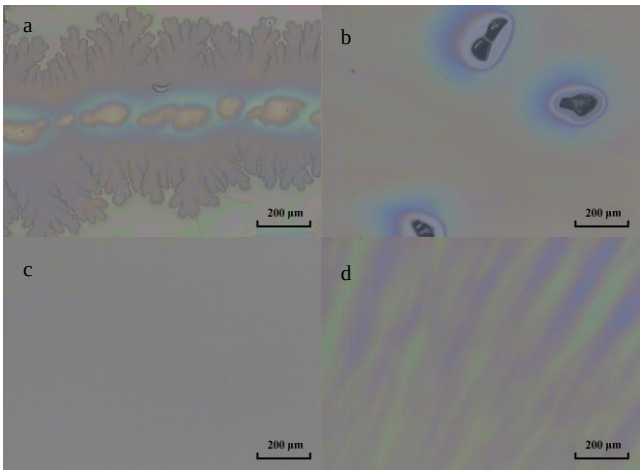

Fig. 2. Optical morphologies of the films (a) H_2O_2-0, (b) H_2O_2-0.35, (c) H_2O_2-0.71 and (d) H_2O_2-0.91

Acid is commonly used as an inhibitor in the sol preparation. For example, Bansal et al. obtained Ta_2O_5 sol from tantalum ethoxide precursor with the addition of HCl [24]. The inhibition mechanism is that the H^+ ions effectively reduce the formation of hydroxides, which are important intermediate products in the sol-gel process. Fig. 3 shows the photoluminescence spectra of the sols with different contents of HNO_3. When excited by the laser at the wavelength of 310 nm, no obvious photoluminescence peaks can be observed from the sol when the HNO_3 content is 2.82. With the HNO_3 content decreases, the photoluminescence peaks of the sol show up and the intensity increases gradually at the wavelength between 350 nm and 450 nm. The intensity of the photoluminescence peak is related to the size of Ta_2O_5 nanoparticles in the sol [25]. If the nanoparticle size is too small, the intensity of the photoluminescence peak would be very weak and even no peaks could be found. With the nanoparticle growth in the sol, the photoluminescence peak intensity continuously strengthened. In this study, when the HNO_3 content is 2.82, the hydrolysis process is very slow and the sol is very stable. Therefore, it is difficult to nucleate and grow nanoparticles in the sol. With the HNO_3 content decrease, the hydrolysis process accelerates and the nanoparticles grow bigger, leading to the stronger photoluminescence intensity.

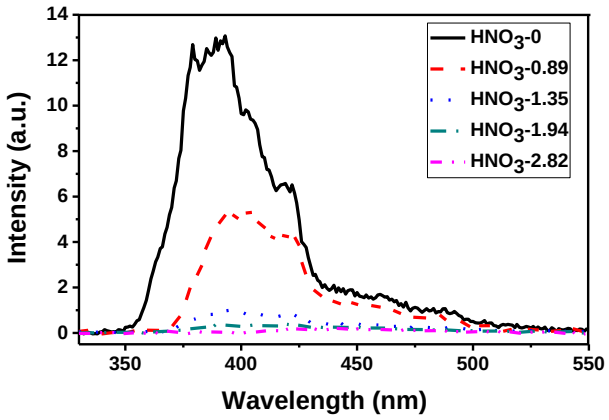

Fig. 3. Photoluminescence spectra of the sols

The oxygen atom of ACAC is surrounded with a lone pair of electrons, which can be combined with an empty orbit of the metal cation through the coordination bond, thereby inhibiting the hydrolysis of the precursor. Fig. 4 shows the transmittance of the sols with different contents of ACAC at the wavelength of 500 nm. To accelerate the reaction process, these three sol groups were aged at room temperature. It is well known that with the extension of aging time, the nanoparticles are formed gradually in the sol, and the transmittance of the sol is getting worse and worse with the continuous growth and agglomeration of the nanoparticles. If there is no ACAC in the sol, $TaCl_5$ hydrolyzes too fast and the nanoparticles grow rapidly, resulting in the precipitation immediately. As shown in Fig.

4, when the ACAC content increases to 0.76, the transmittance decreases significantly after 11 h. It indicates that the nanoparticles in the sol are still unstable and prone to aggregate. However, with the ACAC content increase to 1.36, the sol transmittance decreases only after 93 h, which indicates that the sol is very stable. When the ACAC content increases further to 1.45, the transmittance of the sol changes very slow and there is no significant downward trend. This is because the excessive content of ACAC makes the hydrolyzation and nucleation too hard to form the nanoparticles.

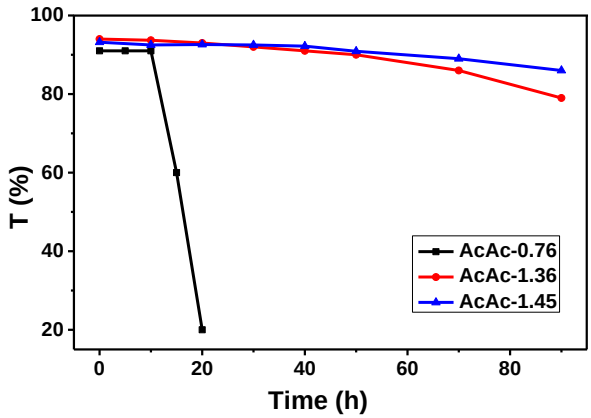

Fig. 4. Transmittance spectra of the sols

The AFM patterns recorded from the films with different ACAC contents are shown in Fig. 5. Fig. 5(a) shows that the film surface is slightly rough with a lot of bumps and the RMS roughness is 0.76 nm when the ACAC content is 0.76. The probable reason is that the nanoparticles in the sol grow fast due to insufficient ACAC, leading to some large particles or aggregates. Fig. 5(b) shows that the film surface is uniform and smooth, and the RMS roughness is 0.62 nm when the ACAC content is 1.36. When ACAC content increases to 1.45, many protuberances appear on the film surface and the RMS roughness of the film increases significantly to 1.00 nm, as shown in Fig. 5(c). As shown in Fig. 4, it is difficult to generate nanoparticles in the sol because of the ACAC excessive content and, so, it is almost impossible to obtain high quality films using the sol.

Fig. 6 shows the weak absorption and LIDT results of the films with different contents of ACAC. It shows that the weak absorption of the films decreases firstly and then increases with the ACAC content increase. When the ACAC content is 0.76, the weak absorption of the film is 22.8 ppm. When the ACAC content rises up to 1.36, the film obtains the smallest weak absorption of 15.1 ppm. With the ACAC content increases further to 1.45, the weak absorption is 22.2 pm. Meanwhile, Fig. 6 shows that with the ACAC content increases, the LIDT of the films decreases after the first rise, which shows an opposite trend compared with the weak absorption. It shows that the LIDT of the film is 21.2 J/cm^2 when the ACAC content is 0.76. When the ACAC content rises up to 1.36, the LIDT of the film raises by 13.7% to 24.1 J/cm^2 compared to that of ACAC-0.76. With the ACAC content increases further to 1.45, the LIDT significantly falls down to 12.0 J/cm^2. Furthermore, it should be noted that the LIDT of the film is the highest and the weak absorption is the lowest when the ACAC content is 1.36.

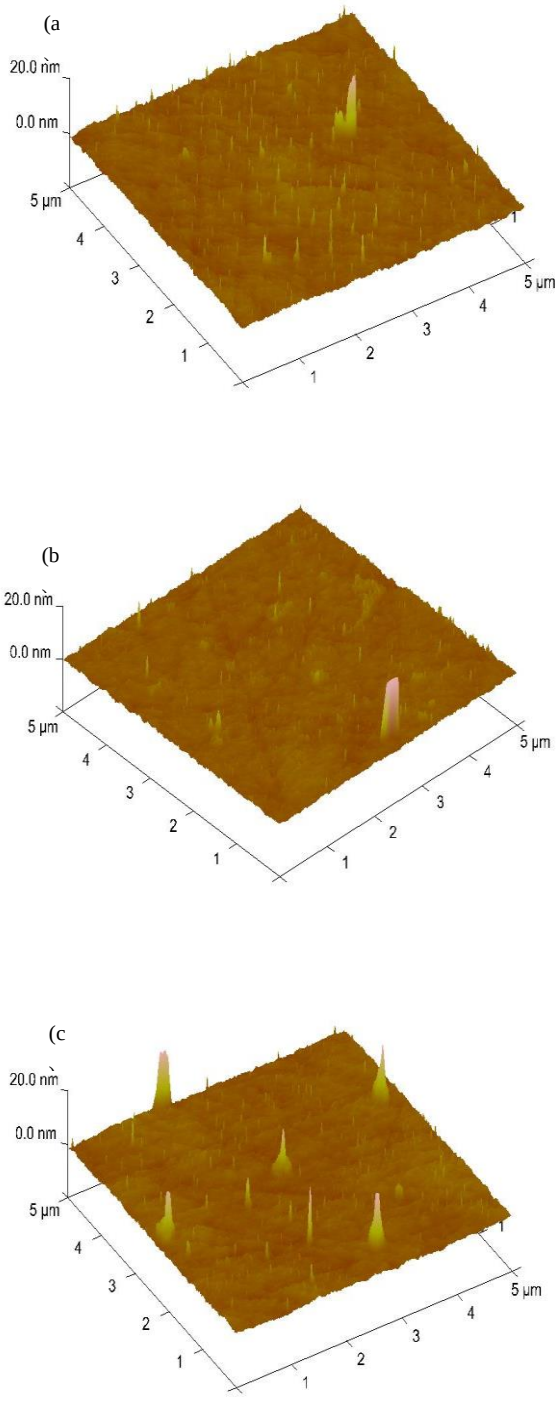

Fig. 5. AFM images of the films (a) ACAC-0.76, (b) ACAC-1.36 and (c) ACAC-1.45

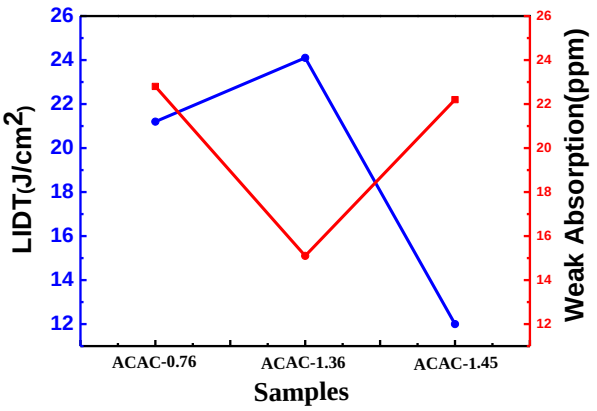

Fig. 6. Weak absorption and LIDT results of the samples

The typical damage morphology of the films with different ACAC contents after laser radiation is shown in Fig. 7. As seen in Fig. 7(a), it is the defect-induced damage mechanism from the standpoint of damage morphologies. It has a damage center and gradually extends to be a circular damage spot. Fig. 7(b) is the enlarged area A in Fig. 7(a), and it shows the obvious spalling phenomenon. This spalling can be attributed to the weak adhesion of sol-gel film with the substrate [20]. Fig. 7(c) is the enlarged image of the area B in Fig. 7(a). The residual trace of a defect which contributed to the ultimate damage can be observed readily. Since the absorbance index of the defect is comparatively much higher than that of the film itself, more energy is absorbed by the defect under laser radiation, leading to the damage trigger point. Near the defect, there are many splash particles which are appeared owing to the remainders of the damaged film after extreme high temperature impact during laser ablation. The highest LIDT of the Ta_2O_5 films obtained in this study is 24.1 J/cm^2. The high laser damage resistance of the films is due to two main factors: (1) the network structure of the sol-gel films. The sol-gel films always have porous network structure with low packing density [26]. Previous results showed that this low packing density was conducive to the formation of a more relaxed film structure more suitable for relieving the expansion of the skeleton when absorbing the laser energy [27-28]. Therefore, it contributes to the high LIDT. (2) No substoichiometric defects in the sol-gel films. The substoichiometric defects such as the oxygen vacancies are very easy to generate in EBE films due to the high temperature deposition. Our previous results showed that oxygen vacancies were the most serious defects decreased the LIDT of Ta_2O_5 films [29-30]. Due to the low temperature deposition route, the sol-gel films are free of substoichiometric defects, which is also beneficial to the improvement of laser damage resistance. In addition, the LIDT of the films decreases to 21.2 J/cm^2 and 12.0 J/cm^2 when the ACAC contents are 0.76 and 1.45, respectively. It is probably attributed to the more defects indicated by the rougher film surface and higher weak absorption, as shown in Figs. 5 and 7.

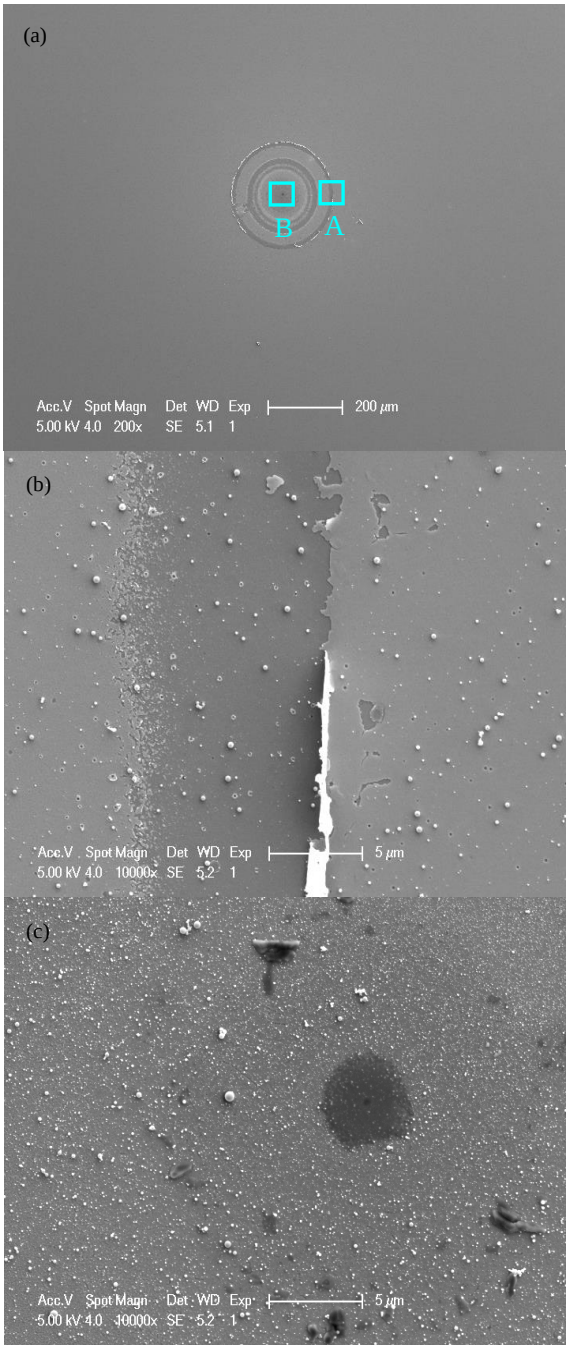

Fig. 7. Typical damage morphologies of the films (a) with ACAC, (b) enlarged area A and (c) enlarged area B

According to the above results, the ranges of the optimal parameters for preparation high LIDT Ta_2O_5 films are proposed as follows: the H_2O_2 contents are in the range of 0.35-0.91, the HNO_3 contents are in the range of 0.89-1.94 and the ACAC contents are in the range of 0.76-1.45. Based on this, we present a pseudo-ternary phase diagram of the system for the preparation of high LIDT Ta_2O_5 films, as shown in Fig. 8. When the contents

of H_2O_2, ACAC and HNO_3 are located in region A in Fig. 8, the synthesized sols are suitable for coating, and the prepared films have high LIDT. The group 10 (ACAC-1.36) in region A has the highest LIDT of 24.1 J/cm^2. When the contents of H_2O_2, ACAC and HNO_3 are located in region B in Fig. 8, the nanoparticles in the sols grow too fast, indicating excessive H_2O_2 and insufficient HNO_3. The group 5 (HNO_3-0) in region B possesses precipitation before the film preparation. When the contents of H_2O_2, ACAC and HNO_3 are located in region C in Fig. 8, the hydrolysis of the sols is too slow, indicating excessive HNO_3. The group 8 (HNO_3-2.82) in region C relates to very difficult nucleation in the sol and, thus, it is unsuitable for the film preparation. When the contents of H_2O_2, ACAC and HNO_3 are located in region D in Fig. 8, it also shows the excruciatingly slow hydrolysis similar to that in region C. The difference between region C and region D is that the former indicates excessive ACAC or insufficient H_2O_2. When the contents of H_2O_2, ACAC and HNO_3 are located in regions E, F and G in Fig. 8, the films can be prepared. However, there are many defects on the film surface and the LIDT is low. For example, the LIDT is only 12.0 J/cm^2 for the film of group 6 (ACAC-0.76) in region E.

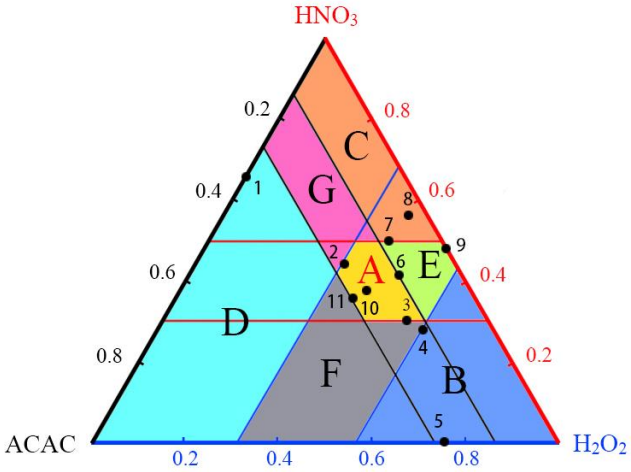

Fig. 8. Pseudo-ternary phase diagram of H_2O_2-HNO_3-ACAC at room temperature. (1: H_2O_2-0; 2: H_2O_2-0.35; 3: H_2O_2-0.71 (HNO_3-0.89); 4: H_2O_2-0.91; 5: HNO_3-0; 6: HNO_3-1.35 (ACAC-0.76); 7: HNO_3-1.94; 8-HNO_3-2.82; 9: ACAC-0; 10: ACAC-1.36; 11: ACAC-1.45)

4. Conclusions

In summary, Ta_2O_5 films are prepared by sol-gel method at different contents of H_2O_2, HNO_3 and ACAC. The results show that with the increase of H_2O_2 content, the nanoparticles in the sol grow faster. However, with the increase of the HNO_3 content, the hydrolysis process is slower and the sol becomes stable. The ACAC shows the similar inhibition effect with HNO_3 on the sols. The highest LIDT of the Ta_2O_5 films obtained in this study is 24.1 J/cm^2. Based on the experimental results, a pseudo-ternary phase diagram of H_2O_2-HNO_3-ACAC system for preparing high LIDT Ta_2O_5 films is proposed, which is helpful to have a better understanding of the preparation process and obtain Ta_2O_5 films with higher laser damage resistance in the future.

Acknowledgement

This work is supported by "the Fundamental Research Funds for the Central Universities (2015XKMS065)", "the Six Talent Peaks Project in Jiangsu Province (2015-XCL-009)" and "Research and Practice on the Teaching Reform of Graduate Education in Jiangsu Province (JGZZ16_080)".

References

[1] Z. Yu, H. He, W. Sun, H. Qi, M. Yang, Q. Xiao, M. Zhu, Opt. Lett. **38**(21), 4308 (2013).
[2] M. Ma, C. Xu, D. Lin, H. Sun, E. Lin, P. Feng, Y. Qiang, D. Li, J. Optoelectron. Adv. M. **19**(3-4), 189 (2017).
[3] C. V. Ramana, S. Utsunomiya, R. C. Ewing, U. Becker, V. V. Atuchin, V. Sh. Aliev, V. N. Kruchinin, Appl. Phys. Lett. **92**(1), 011917 (2008).
[4] C. Xu, J. Jia, D. Yang, H. Fan, Y. Qiang, J. Liu, G. Hu, D. Li, J. Appl. Phys. **116**, 053102 (2014).
[5] P. Shang, S. Xiong, L. Li, Appl. Surf. Sci. **285**, 713 (2013).
[6] C. Xu, D. Lin, J. Niu, Y. Qiang, D. Li, C. Tao, Chin. Phys. Lett. **32**, 088102 (2015).
[7] V. V. Atuchin, J.-Z. Grivel, Z. Zhang, Chem. Phys. **360**, 74 (2009).
[8] C. Xu, D. Li, H. Fan, J. Deng, J. Qi, P. Yi, Y. Qiang, Thin Solid Films. **580**, 12 (2015).
[9] C. V. Ramana, V. V. Atuchin, V. G. Kesler, V. A. Kochubey, L. D. Pokrovsky, V. Shutthanandan, U. Becker, R. C. Ewing, Appl. Surf. Sci. **253**, 5368 (2007).
[10] V. A. Shvets, V. Sh. Aliev, D. V. Gritsenko, S. S. Shaimeev, E. V. Fedosenko, S. V. Rykhlitski, V. V. Atuchin, V. A. Gritsenko, V. M. Tapilin, H. Wong, J. Non-Cryst. Solids **354**, 3025 (2008).
[11] V. V. Atuchin, A. V. Kalinkin, V. A. Kochubey, V. N. Kruchinin, R. S. Vemuri, C. V. Ramana, J. Vac. Sci. Technol. A **29**, 021004 (2011).
[12] V. V. Atuchin, V. N. Kruchinin, Y. H. Wong, K. Y. Cheong, Mater. Lett. **105**, 72 (2013).
[13] V. M. Kalygina, I. S. Egorova, I. A. Prudaev, O. P. Tolbanov, V. V. Atuchin, Microwave Opt. Technol. Lett. **58**, 1113 (2016).
[14] C. Xu, Q. Xiao, J. Ma, Y. Jin, J. Shao, Z. Fan, Appl. Surf. Sci. **254**(20), 6554 (2008).
[15] C. Xu, D. Lin, P. Feng, D. Li, H. Fan, J. Qi, J. Niu, Y.

Qiang, J. Optoelectron. Adv. M. **17**(11-12), 1739 (2015).
[16] J. Yao, H. Li, Z. Fan, Y. Tang, Y. Jin, Y. Zhao, H. He, J. Shao, Chin. Phys. Lett. **24**, 1964 (2007).
[17] D. Grosso, P. Sermon, Thin Solid Films **368**, 116 (2000).
[18] T. Ohya, M. Kabata, T. Ban, Y. Ohya, Y. Takahashi, J. Sol-Gel Sci. Technol. **25**, 43 (2002).
[19] M. J. Wolf, S. Roitsch, J. Mayer, A. Nijmeijer, H. J. M. Bouwmeester, Thin Solid Films **527**, 354 (2013).
[20] C. Xu, P. Yi, H. Fan, J. Qi, S. Yang, Y. Qiang, J. Liu, D. Li, Appl. Surf. Sci. **309**, 194 (2014).
[21] H. He, X. Li, S. Fan, J. Shao, Y. Zhao, Z. Fan, Proc. SPIE 5991, F59912 (2005).
[22] Y. Zhao, Y. Wang, H. Gong, J. Shao, Z. Fan, Appl. Surf. Sci. **210**, 353 (2003).
[23] ISO 11254-1:2000: Lasers and laser-related equipment-determination of laser-induced damage threshold of optical surfaces. Part 1. 1-on-1 test.
[24] F. Duminica, F. Maury, S. Abisset, Thin Solid Films **515**, 7732 (2007).
[25] C. Xu, D. Li, H. Fan, J. Qi, J. Deng, S. Yang, P. Yi, Y. Qiang, Appl. Surf. Sci. **344**, 137 (2015).
[26] K. Yoshida, T. Yabe, H. Yoshida, J. Appl. Phys. **60**, 1545 (1986).
[27] F. Chi, L. Yan, H. Lv, C. Wang, X. Yuan, Thin Solid Films **519**, 2483 (2011).
[28] X. Li, M. Gross, B. Oreb, J. Shen, J. Phys. Chem. C. **116**, 18367 (2012).
[29] C. Xu, M. Ma, H. Sun, D. Lin, P. Feng, J. Qi, Y. Qiang, Dawei Li, C. Tao, Optoelectron. Adv. Mat. **9**(11-12), 1337 (2015).
[30] C. Xu, P. Yi, H. Fan, J. Qi, Y. Qiang, J. Liu, C. Tao, D. Li, Appl. Surf. Sci. **289**, 141 (2014).

*Corresponding author: xucheng@cumt.edu.cn